

## Covid-19 Diagnosis by Wavelet Entropy and Extreme Learning Machine

Xue Han<sup>1,\*</sup>, Zuojin Hu<sup>2</sup> and William Wang<sup>3</sup>

<sup>1</sup>Nanjing Normal University of Special Education, Nanjing, Jiangsu, 210000, China

<sup>2</sup>Nanjing Normal University of Special Education, Nanjing, Jiangsu, 210000, China

<sup>3</sup>Waynesburg University, Waynesburg, PA 15370, USA

### Abstract

In recent years, COVID-19 has spread rapidly among humans. Chest CT is an effective means of diagnosing COVID-19. However, the diagnosis of CT images still depends on the doctor's visual judgment and medical experience. This takes a certain amount of time and may lead to misjudgment. In this paper, a new algorithm for automatic diagnosis of COVID-19 based on chest CT image data was proposed. The algorithm comprehensively uses WE to extract image features, uses ELM for training, and finally passes k-fold CV validation. After evaluating and detecting performance on 296 chest CT images, our proposed method is superior to state-of-the-art approaches in terms of sensitivity, specificity, precision, accuracy, F1, MCC and FMI.

**Keywords:** COVID-19, diagnosis, Wavelet Entropy, Extreme Learning Machine, k-fold cross validation.

Received on 21 June 2022, accepted on 09 August 2022, published on 11 August 2022

Copyright © 2022 Xue Han *et al.*, licensed to EAI. This is an open access article distributed under the terms of the [Creative Commons Attribution license](#), which permits unlimited use, distribution and reproduction in any medium so long as the original work is properly cited.

doi: 10.4108/eetel.v8i1.2504

### 1. Introduction

On February 11, 2020, the Director-General of the World Health Organization, Tedros Adhanom Ghebreyesus, announced in Geneva, Switzerland, that the pneumonia caused by the novel coronavirus was named "COVID-19" [1]. On March 11, the World Health Organization considered the current COVID-19 outbreak to be called a global pandemic [2]. As of 20:11 CEST on May 23, there have been 52,278,3196 confirmed cases of novel coronary pneumonia in the world and 6,276,210 deaths.

Chest computed tomography (CT) is one of the commonly used monitoring methods. Chest CT in patients with COVID-19 usually shows bilateral lower lung ground-glass opacity (GGO) [3]. From the CT scans of 93 COVID-19 patients, Wang et al. found that the detection rate of ground glass shadows in normal patients (79.5%) was higher than that in critically ill patients (55%), and the detection rate of consolidation shadows in critically ill patients (90%) was higher in normal patients (52.1%) [4]. Bernheim et al. found

from CT of 121 patients with COVID-19 that the detection rate of ground-glass opacity and consolidation opacity increased with the increase of the number of days of onset [5]. During the course of treatment, the treatment effect was good, and the lung CT also showed good performance. On the contrary, the CT showed that the situation deteriorated [6-8]. Compared with viral test, CT can help doctors to better judge the critical condition of the disease, the duration of the disease, and the effect of treatment [9-11].

Radial basis function neural network (RBFNN) is a feedforward neural network with a single hidden layer, which consists of an input layer, a single hidden layer (radial basis layer), and an output layer (linear). Universal approximator, best-approximation property, and optimality are the features of RBFNN. RBFNN can choose different activation functions of the hidden layer according to different needs. Lu et al. [12] combined wavelet entropy and RBFNN to classify brain MR images into pathological and healthy. But, it is difficult for technicians to understand the weights/biases of RBFNN. Moreover, this method can only perform single classification of images, not multi-class classification.

\*Xue Han. Email: [snow\\_3@163.com](mailto:snow_3@163.com)

K-ELM is a variant of ELM. It can provide different kernel functions for optimization, regression and classification. Lu et al. [13] used wavelet entropy as the features and K-ELM as a classifier to classify images as pathological or healthy. The hard part is interpreting the entropy values or the weights/biases of K-ELM.

Extreme learning machine (ELM) is a single hidden layer neural network learning method. ELM can solve regression and classification problems. Sometimes it is used in combination with the Bat algorithm (BA) to solve the problem of redundant nodes due to randomly parameters of the hidden layer, and to optimize the weight/bias. Lu et al. [14] calculated the wavelet entropies of the subbands as features, and trained a bat algorithm optimized extreme learning machine (BA-ELM) to identify images of pathological brains. However, doctors and technicians have difficulty in understanding the values of entropy and the weights of the classifier.

For chest CT images of COVID-19 patients, this study proposes a method to screen data images based on wavelet entropy, use extreme learning machine algorithm [15, 16] to obtain data models, and then evaluate the performance indicators of data models through  $k$ -fold cross-validation. It aims to obtain more accurate chest CT images [17] of patients without redundancy, so as to help clinicians make more accurate judgments of patients' conditions. Compared with other algorithms, this paper adopts an improved algorithm of traditional machine learning algorithm, which overcomes the disadvantages of traditional machine learning, makes the implementation simpler and the result more accurate.

The parts of this paper are organized as follows: Section 2 elaborates the selection method of the dataset. Section 3 describes how wavelet entropy analyzes image signals, applies extreme learning machine algorithms, and  $k$ -fold cross-validation methods to train and validate sample data on small datasets. Section 4 conducts the experimental design, gives the experimental results and discusses them. Section 5 summarizes the full text.

## 2. Dataset

Using a Philips Ingenuity 64 row spiral CT machine, we randomly selected 66 healthy subjects, including 31 males and 35 females, from healthy people, and acquired 148 chest CT images; 66 patients with COVID-19 were randomly selected, including 41 males and 25 females also acquired 148 chest CT images. The subjects were in a supine position, with both upper limbs lifted up, holding their breath after deep inhalation, and a CT scan was performed from the thoracic inlet to the costal diaphragm angle. scanning layer thick layer spacing is 3 mm., and the CT image resolution was  $1024 \times 1024$  [18].

## 3. Methodology

### 3.1. Wavelet Entropy

Compared with Fourier transform [19], wavelet transform (WT) [20, 21] emphasizes localized analysis in time and frequency [22], and multi-scale refinement of signals through scaling and translation. Finally, time refinement is achieved at high frequencies, and frequency refinement at low frequencies. Wavelet analysis is an important tool for dealing with unstable signals.

The "information entropy" proposed by Shannon is the average amount of information after excluding information redundancy [23]. The average uncertainty of the information  $H(x)$  is the statistical average of the uncertainty of the individual information symbols  $H(x_i)$ , the information entropy is defined as shown in Equation (1).

$$H(x) = H(x_1, x_2, \dots, x_n) = - \sum_{i=1}^n p(x_i) \log p(x_i) \quad (1)$$

There are  $n$  information symbols  $x_i (i=1, \dots, n)$  in total, and the uncertainty of each information symbol  $x_i$  is  $p(x_i)$ . The greater the entropy, the greater the uncertainty of the information, and the more the amount of information [24].

Applying the theory of information entropy to wavelet analysis, the wavelet entropy can be obtained. Signals are refined in time and frequency by WT [25, 26], and WE is used as the quantitative evaluation standard for local analysis at each resolution. WE ( $L$ ) is define as shown in Equation (2).

$$L = - \sum_{j=1}^m q_j \log q_j \quad (2)$$

The signal after wavelet transformation [27, 28] is distributed in  $m$  resolutions, and  $q_j$  is the relative energy of each resolution. Remove the part with small entropy value, that is, the part with less redundancy and information, and keep the part with large entropy value, that is, the part with large uncertainty and more information. In this way, the key feature parts of the signal are obtained as the input of the dataset. Deep learning methods [29] are not used because of the small-size dataset.

### 3.2. Extreme Learning Machine

Feedforward neural network is one of the most widely used neural networks today. It consists of input layer, hidden layer and output layer [30]. Each layer consists of several neurons, each neuron receives the output of the previous layer as input, and then generates output to the next layer [31], which belongs to one-way propagation [32]. According to the number of hidden layers, it is divided into single-layer feed-forward neural network and multi-layer feed-forward neural network.

Extreme Learning Machine (ELM) [33] is a learning algorithm for a single-layer feedforward neural network (SLFN), which is an improvement on the back-propagation (BP) algorithm [34]. Based on the theory that when the activation function in the hidden layer of a single-layer feedforward neural network [35] is infinitely differentiable, the input weights and the bias of the hidden layer can be randomly selected [36]. No adjustment is required, independent of the training data, it can still accurately learn multiple different observations, and the learning speed is faster than the traditional back-propagation algorithm [37], and it tends to achieve the minimum training error and minimum weight norm. Bartlett's [38] theory on the generalization performance of feedforward neural network shows that the smaller the training error of the current feedforward neural network [39, 40], the smaller the weight norm, the better the generalization performance of the network.

An SLFN with  $n$  nodes  $(x_i, y_i)$  in the input layer, the input matrix is  $x_i=[x_{i1}, x_{i2}, \dots, x_{in}]^T \in \mathbf{R}^n$ , and the output matrix is  $y_i=[y_{i1}, y_{i2}, \dots, y_{im}]^T \in \mathbf{R}^m$ , its hidden layer has  $l$  hidden layer nodes, which can be expressed as (3) [36]:

$$y_j = \sum_{i=1}^l \beta_i g(w_i \cdot x_j + b_i), \quad j = 1, \dots, n \quad (3)$$

$g(x)$  is activation function.  $\beta=[\beta_{1l}, \beta_{12}, \dots, \beta_{lm}]^T$  is the weight from the  $i$ th hidden layer node mapped to the output layer node.  $w_i=[w_{i1}, w_{i2}, \dots, w_{in}]^T$  is the weight from the input layer node mapped to the  $i$ th hidden layer node.  $b_i$  is the threshold of the  $i$ th hidden node.

The ELM algorithm is summarized as:

- (1) The input weight  $w_i$  and bias  $b_i$  are randomly assigned to  $l$  hidden layer nodes.
- (2) The hidden layer output matrix  $H$  is calculated,  $H$  is expressed as (4):

$$H(w_1, \dots, w_l, b_1, \dots, b_l, x_1, \dots, x_n) = \begin{bmatrix} g(w_1 \cdot x_1 + b_1) & \dots & g(w_l \cdot x_1 + b_l) \\ \vdots & \ddots & \vdots \\ g(w_1 \cdot x_n + b_1) & \dots & g(w_l \cdot x_n + b_l) \end{bmatrix} \quad (4)$$

- (3) The output weight matrix  $\beta$  is calculated,  $\beta$  is expressed as (5):

$$\beta = \begin{bmatrix} \beta_1^T \\ \vdots \\ \beta_l^T \end{bmatrix} \quad (5)$$

Table 1 is a pseudocode of ELM:

Table 1. A pseudocode of ELM

Input: $n$ input layer nodes, $x_i=[x_{i1}, x_{i2}, \dots, x_{in}]^T$
$l$ hidden layer nodes
activation function $g(x)$
for $i=1:l$
random initialization weight $w_i$ and bias $b_i$
calculate $H_i$
calculate $\beta$
end
Obtain the hidden layer output matrix $H$
Obtain the output weight matrix $\beta$ .

### 3.3. $k$ -fold Cross Validation

The purpose of cross-validation is to solve the situation of insufficient data volume of the dataset [41, 42]. In simple cross-validation, the original data set is divided into two parts, one is the training set and the other is the validation set [43]. In this way, the data can only be used as training data or validation data once, and it is not fully utilized; the validation results will also vary depending on the standard by which the original data is divided.

$k$ -fold cross-validation can solve the shortcomings of simple cross-validation. It solves the problem of selectivity bias of results due to the selection of local data as the validation set in simple cross-validation, and has good generalization ability [44]. The original dataset is divided into  $k$  similarly sized subsets (folds) [45]. Each time the data model is trained, one of the folds is used as the validation set, and the other folds are used as the training set [46, 47], and the performance value  $s_i$  of the trained data model is obtained after verification. In this way, the training iteration of the data model is performed  $k$  times [48], and each fold will be used as a validation set once and  $k-1$  times as a training set [49]. Finally, the performance evaluation result of the data model is the average value  $s$  of the  $k$  performance values, as shown in formula (6). The method of  $k$ -fold cross validation is illustrated in Figure 1. [44]

$$s = \frac{1}{k} \sum_{i=1}^k s_i \quad (6)$$

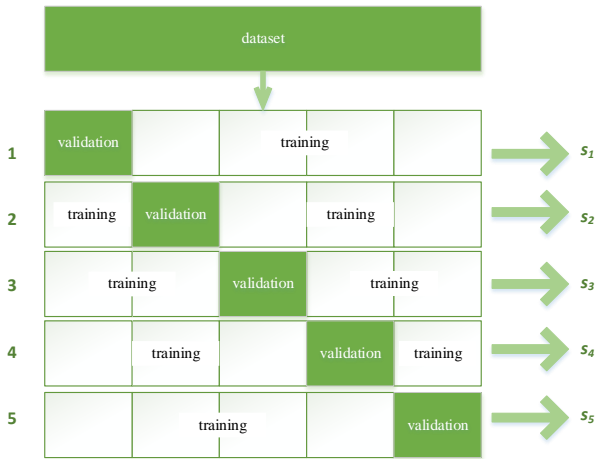


Figure 1.  $k$ -fold cross validation (with  $k=5$ )

## 4. Experiment Results and Discussions

### 4.1. WE Results

Figure 2 is a wavelet decomposition sample of a subject's lung CT. The CT image is decomposed by a low-pass filter  $l$  and a high-pass filter  $h$ , and four sub-bands are generated:  $lll$ ,  $lh1$ ,  $hl1$ ,  $hh1$ . (a) is the 1-level decomposition result. The subband  $lll$  is further decomposed in the same way to obtain  $ll2$ ,  $lh2$ ,  $hl2$ , and  $hh2$ . (b) is the 2-level decomposition result. Decompose  $ll2$  to get  $ll3$ ,  $lh3$ ,  $hl3$ ,  $hh3$ . (c) is the 3-level decomposition result. Decompose  $ll3$  to get  $ll4$ ,  $lh4$ ,  $hl4$ ,  $hh4$ . (d) is the 4-level decomposition result. After the 4-level decomposition, the details in the CT image can be observed more clearly.

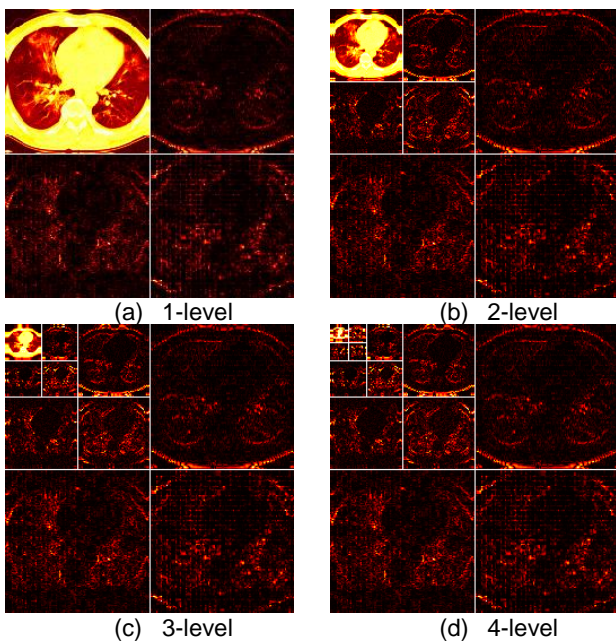


Figure 2. different levels of wavelet decomposition

### 4.2. Statistical Results

Table 2 is the result of running ten  $k$ -fold cross-validation ( $k=10$ ). Sensitivity refers to the percentage of positive samples detected in patient samples (including true positives and false negatives), indicating the rate of no missed diagnosis. Specificity refers to the percentage of negative samples detected in healthy samples (including true negatives and false positives), indicating the non-misdiagnosis rate. Precision refers to the percentage of true positive samples detected in positive patients (both true positives and false positives). Accuracy refers to the percentage of true positive samples and true negative samples detected in the total samples. The mean(M) of the ten running results is higher than 75%, and the standard deviation(SD) is basically not higher than 2.5. The values of FMI in Table 2 are basically above +0.75, and the MCC values are all around +0.5. The monitoring results of the model are better than random monitoring.

### 4.3. Comparison to State-of-the-art Approaches

We compared our WE-ELM algorithm with state-of-the-art approaches: RBFNN, K-ELM, ELM-BA. As shown in Table 3 and Figure 3, in the detection of precision, accuracy and F1 for COVID-19, the best is WE-ELM (Ours), the second is RBFNN, the third is ELM-BA, and the last is K-ELM. In the detection of sensitive for COVID-19, the best is WE-ELM (Ours), the second is RBFNN, the third is K-ELM, and the last is E-LMBA. In the detection of specific for COVID-19, the best is WE-ELM (Ours), the second is ELM-BA, the third is RBFNN, and the last is K-ELM. Furthermore, the MCC value of WE-ELM is  $53.35 \pm 2.26\%$ , and the FMI value of WE-ELM is  $76.39 \pm 1.41\%$ . So, WE-ELM (Ours) presents better performance than the current method in the detection of COVID-19.

## 5. Conclusions

This paper proposes a computer vision-based method for diagnosing Covid-19 by detecting lung CT images. The method consists of three parts: WE extracts image features, ELM is used for training, and  $k$ -CV is used as data validation. It can be seen through experiments that after 10 times 10-fold CV, the MCC value of our method is  $53.35 \pm 2.26\%$ , and the performance of other indicators is also better than the other three state-of-the-art approaches (see Section 4.3). Compared with the existing diagnostic methods (see Section 4.3), the WE-ELM algorithm proposed in this paper has better performance than other methods.

The algorithm proposed in this paper for diagnosing 2019-nCoV has two shortcomings: firstly, WE was extracted, and only the features of health or pathology were identified, and

there are no features for further classification of pathology. Secondly, the values of MCC are only about 50%, which need to be improved and further optimized.

In future studies, according to the differences of chest CT of COVID-19 patients, we will conduct a classification study of COVID-19 pathology based on computer vision. Second,

the WE-ELM proposed in this paper can be applied to other computer vision-based recognition, such as emotion recognition, gesture recognition, etc. Third, we will continue to collect more data, and test the deep learning method when the amount of data is sufficient.

Table 2. Ten runs of 10-fold cross validation

Run	Sensitivity	Specificity	Precision	Accuracy	F1	MCC	FMI
1	77.70	77.70	77.70	77.70	77.70	55.41	77.70
2	76.35	79.05	78.47	77.70	77.40	55.43	77.40
3	78.38	77.03	77.33	77.70	77.85	55.41	77.85
4	72.30	77.70	76.43	75.00	74.31	50.07	74.33
5	74.32	79.73	78.57	77.03	76.39	54.13	76.42
6	73.65	78.38	77.30	76.01	75.43	52.09	75.45
7	78.38	74.32	75.32	76.35	76.82	52.75	76.84
8	72.97	77.03	76.06	75.00	74.48	50.04	74.50
9	72.97	79.05	77.70	76.01	75.26	52.12	75.30
10	78.38	77.70	77.85	78.04	78.11	56.08	78.11
MSD	75.54	77.77	77.27	76.66	76.38	53.35	76.39
	±2.54	±1.51	±1.04	±1.14	±1.42	±2.26	±1.41

Table 3. Comparison with state-of-the-art methods.

Method	Sensitivity	Specificity	Precision	Accuracy	F1	MCC	FMI
RBFNN [12]	66.89	75.47	73.23	71.18	69.88	42.56	69.97
	±2.43	±2.53	±1.48	±0.80	±1.08	±1.61	±1.04
K-ELM [13]	58.78	60.27	59.73	59.53	59.19	19.09	59.22
	±3.36	±3.89	±1.68	±1.42	±1.86	±2.83	±1.79
ELM-BA [14]	56.55	76.22	70.45	66.39	62.69	33.46	63.09
	±2.99	±2.56	±1.61	±1.05	±1.76	±2.07	±1.60
WE-ELM (Ours)	75.54	77.77	77.27	76.66	76.38	53.35	76.39
	±2.54	±1.51	±1.04	±1.14	±1.42	±2.26	±1.41

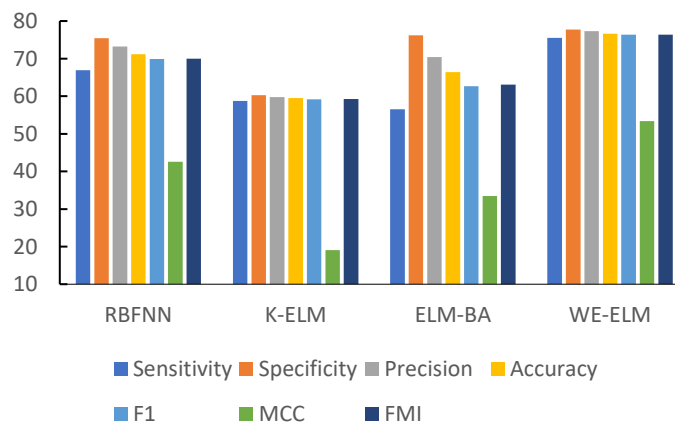


Figure 3. Bar plot of comparison results

## References

- [1] Kovacs, K.D., Determination of the human impact on the drop in NO<sub>2</sub> air pollution due to total COVID-19 lockdown using Human-Influenced Air Pollution Decrease Index (HIAPDI)\*. *Environmental Pollution*, 2022. 306: Article ID. 119441
- [2] Diaz, A., C. Esparcia, and R. Lopez, The diversifying role of socially responsible investments during the COVID-19 crisis: A risk management and portfolio performance analysis. *Economic Analysis and Policy*, 2022. 75: p. 39-60
- [3] Farhangnia, P., S. Dehrouyeh, A.R. Safdarian, S.V. Farahani, M. Gorgani, N. Rezaei, M. Akbarpour, and A.A. Delbandi, Recent advances in passive immunotherapies for COVID-19: The Evidence-Based approaches and clinical trials. *International Immunopharmacology*, 2022. 109: Article ID. 108786
- [4] J. Wang, Z.X., J. Wang, R. Feng, Y. An, W. Ao, Y. Gao, X. Wang, Z. Xie, CT characteristics of patients infected with 2019 novel coronavirus: association with clinical type. *Clinical Radiology*, 2020(75): p. 408-414
- [5] A. Bernheim, X.M., M. Huang, Y. Yang, Z. A. Fayad, N. Zhang, et al., Chest CT findings in coronavirus disease-19 (COVID-19): relationship to duration of infection. *Radiology*, 2020: p. 295
- [6] Ong, S., C. Pascoe, Z. Ballock, S. Sengupta, D. Murphy, and N. Lawrentschuk, Long Term follow-up of men having a PSMA PET-CT for biochemical progression of prostate cancer - Is a negative scan prognostic? *BJU International*, 2022. 129: p. 155-155
- [7] Sahba, S., A. Huurnink, J.M. van den Berg, B. Tuitert, S.J. Vastert, and G.W. ten Tusscher, Systemic Juvenile Idiopathic Arthritis in two children; case report on clinical course, challenges in diagnosis and the role of FDG-PET/CT-scan. *Clinical Case Reports*, 2022. 10(6): Article ID. e05900
- [8] Halily, S., B. Abdulhakeem, Y. Oukessou, S. Rouadi, R. Abada, M. Roubal, and M. Mahtar, CT scan findings impact on hearing thresholds in otosclerosis: A study of 108 patients. *Annals of Medicine and Surgery*, 2022. 77: Article ID. 103716
- [9] Das, S.S., D. Malik, G. Khanna, I.B. Sen, and R. Patir, F-18-Labeled WBC PET/CT Scan in a Case of Recurrent Glioblastoma Multiforme, Presented as Pyrexia of Unknown Origin. *Clinical Nuclear Medicine*, 2022. 47(7): p. E500-E502
- [10] Ingvardson, G.T., D. Muter, and B.P. Foley, Purse of medieval silver coins from royal shipwreck revealed by X-ray microscale Computed Tomography (?CT) scanning. *Journal of Archaeological Science-Reports*, 2022. 43: Article ID. 103468
- [11] Watt, I., E. Holden, F. Waldie, J. Bhattacharya, R. Devin, and J. Wu, Utility of CT head scan post inpatient fall in older adults. *Australasian Journal on Ageing*, 2022. 41: p. 25-25
- [12] Zhihai Lu, S.L., Ge Liu, Yudong Zhang, Jianfei Yang, Preetha Phillips, A Pathological Brain Detection System Based on Radial Basis Function Neural Network. *Journal of Medical Imaging and Health Informatics*, 2016. 6(5): p. 1218-1222
- [13] Siyuan Lu, Z.L., Jianfei Yang, Ming Yang, Shuihua Wang, A pathological brain detection system based on kernel based ELM. *Multimedia Tools and Applications*, 2018. 77(3): p. 3715-3728
- [14] Siyuan Lu, X.Q., Jianpin Shi, Na Li, Zhi-Hai Lu, Peng Chen, Meng-Meng Yang, Fang-Yuan Liu, Wen-Juan Jia, Yudong Zhang, A Pathological Brain Detection System based on Extreme Learning Machine Optimized by Bat Algorithm. *CNS & Neurological Disorders - Drug Targets*, 2017. 16(1): p. 23-29
- [15] Ahmadipour, M., M.M. Othman, M. Alrifayeh, R. Bo, and C.K. Ang, Classification of faults in grid-connected photovoltaic system based on wavelet packet transform and an equilibrium optimization algorithm-extreme learning machine. *Measurement*, 2022. 197: Article ID. 111338
- [16] Choi, S. and D. Harrison, Combined 7-Tesla MRI and clinical features in Random Forests and eXtreme Gradient Boost machine learning algorithms for MS progression status classification. *Multiple Sclerosis Journal*, 2022. 28(1\_SUPPL): p. 137-138
- [17] Zhang, Y.-D., A five-layer deep convolutional neural network with stochastic pooling for chest CT-based COVID-19 diagnosis. *Machine Vision and Applications*, 2021. 32: Article ID. 14
- [18] Wang S , W.X., Zhang Y D , et al., Diagnosis of COVID-19 by Wavelet Renyi Entropy and Three-Segment Biogeography-Based Optimization. *International Journal of Computational Intelligence Systems*, 2020(13(1)): p. 1332-1344
- [19] Liu, G., Computer-aided diagnosis of abnormal breasts in mammogram images by weighted-type fractional Fourier transform. *Advances in Mechanical Engineering*, 2016. 8(2): Article ID. 11
- [20] Hussain, N., M. Hasanzade, and D.W. Breiby, Performance comparison of wavelet families for noise reduction and intensity thresholding in Fourier Ptychographic microscopy. *Optics Communications*, 2022. 519: Article ID. 128400
- [21] Chatterjee, S., Sparsity-based modified wavelet de-noising autoencoder for ECG signals. *Signal Processing*, 2022. 198: Article ID. 108605
- [22] Zhang, Y.D., L.N. Wu, G. Wei, and S.H. Wang, A novel algorithm for all pairs shortest path problem based on matrix multiplication and pulse coupled neural network. *Digital Signal Processing*, 2011. 21(4): p. 517-521
- [23] Hou, X.-X., Alcoholism detection by medical robots based on Hu moment invariants and predator-prey adaptive-inertia chaotic particle swarm optimization. *Computers and Electrical Engineering*, 2017. 63: p. 126-138
- [24] Li, P. and G. Liu, Pathological Brain Detection via Wavelet Packet Tsallis Entropy and Real-Coded Biogeography-based Optimization. *Fundamenta Informaticae*, 2017. 151(1-4): p. 275-291
- [25] Valogiannis, G. and C. Dvorkin, Towards an optimal estimation of cosmological parameters with the wavelet scattering transform. *Physical Review D*, 2022. 105(10): Article ID. 103534
- [26] Takano, D., T. Minamoto, and Ieee. Feature extraction method for early-stage colorectal cancer using dual-tree complex wavelet packet transform. in *International Conference on Wavelet Analysis and Pattern Recognition (ICWAPR)*. 2021. *Electr Network: IEEE*. p. 1-4
- [27] Hiramatsu, T., T. Manamoto, and Ieee. Detection of maliciously blurred image portions using dyadic wavelet transform and jensen-shannon divergence. in *International Conference on Wavelet Analysis and Pattern Recognition (ICWAPR)*. 2021. *Electr Network*. p. 5-10
- [28] Yamni, M., H. Karmouni, M. Sayyouri, and H. Qjidaa, Robust audio watermarking scheme based on fractional Charlier moment transform and dual tree complex wavelet transform. *Expert Systems with Applications*, 2022. 203: Article ID. 117325
- [29] Wang, S.-H., DenseNet-201-Based Deep Neural Network with Composite Learning Factor and Precomputation for Multiple Sclerosis Classification. *ACM Trans. Multimedia Comput. Commun. Appl.*, 2020. 16(2s): p. Article 60
- [30] Ganesan, A. and S.M. Santhanam, A novel feature descriptor based coral image classification using extreme learning machine with ameliorated chimp optimization algorithm. *Ecological Informatics*, 2022. 68: Article ID. 101527

- [31] Ghoggali, N., F. Douak, and W. Ghoggali, Towards a NIR Spectroscopy ensemble learning technique competing with the standard ASTM-CFR: An optimal boosting and bagging extreme learning machine algorithms for gasoline octane number prediction. *Optik*, 2022. 257: Article ID. 168813
- [32] Lu, S., Cerebral Microbleed Detection via Convolutional Neural Network and Extreme Learning Machine. *Frontiers in Computational Neuroscience*, 2021. 15: Article ID. 738885
- [33] Gutierrez, D.A., F.S. Lasheras, V.M. Sanchez, S.L.S. Gomez, V. Moreno, F. Moratalla-Navarro, and A.J.M. de la Torre, A New Algorithm for Multivariate Genome Wide Association Studies Based on Differential Evolution and Extreme Learning Machines. *Mathematics*, 2022. 10(7): Article ID. 1024
- [34] Zhang, Y.-D., G. Zhao, J. Sun, X. Wu, Z.-H. Wang, H.-M. Liu, V.V. Govindaraj, T. Zhan, and J. Li, Smart pathological brain detection by synthetic minority oversampling technique, extreme learning machine, and Jaya algorithm. *Multimedia Tools and Applications*, 2017. 77(17): p. 22629-22648
- [35] Wei, G., Color Image Enhancement based on HVS and PCNN. *SCIENCE CHINA Information Sciences*, 2010. 53(10): p. 1963-1976
- [36] Guang-Bin Huang, Q.-Y.Z., Chee-Kheong Siew, Extreme learning machine: Theory and applications. *Neurocomputing*, 2006(70): p. 489-501
- [37] Wu, X., Smart detection on abnormal breasts in digital mammography based on contrast-limited adaptive histogram equalization and chaotic adaptive real-coded biogeography-based optimization. *Simulation*, 2016. 92(9): p. 873-885
- [38] Bartlett, P.L., The sample complexity of pattern classification with neural networks: the size of the weights is more important than the size of the network. *IEEE Trans. Inf. Theory*, 1998(44(2)): p. 525-536
- [39] Nikzad, S. and A. Ebrahimi, Two person interaction recognition based on a dual-coded modified metacognitive (DCMMC) extreme learning machine. *Turkish Journal of Electrical Engineering and Computer Sciences*, 2022. 30(4): p. 1621-1636
- [40] Khan, A.R., T. Saba, T. Sadad, and S.P. Hong, Cloud-Based Framework for COVID-19 Detection through Feature Fusion with Bootstrap Aggregated Extreme Learning Machine. *Discrete Dynamics in Nature and Society*, 2022. 2022: Article ID. 3111200
- [41] Akbarian, S., C.Y. Xu, W.J. Wang, S. Ginns, and S. Lim, Sugarcane yields prediction at the row level using a novel cross-validation approach to multi-year multispectral images. *Computers and Electronics in Agriculture*, 2022. 198: Article ID. 107024
- [42] de Bruin, S., D.J. Brus, G.B.M. Heuvelink, T.V. Tengbergen, and A. Wadoux, Dealing with clustered samples for assessing map accuracy by cross-validation. *Ecological Informatics*, 2022. 69: Article ID. 101665
- [43] Li, Y., Detection of Dendritic Spines using Wavelet Packet Entropy and Fuzzy Support Vector Machine. *CNS & Neurological Disorders - Drug Targets*, 2017. 16(2): p. 116-121
- [44] Soper, D.S., Greed Is Good: Rapid Hyperparameter Optimization and Model Selection Using Greedy k-Fold Cross Validation. *Electronics*, 2021. 10(16): p. 1973
- [45] Peng, B., Y.-X. Liang, J. Yang, and K. So, Image processing methods to elucidate spatial characteristics of retinal microglia after optic nerve transection. *Scientific Reports*, 2016. 6: Article ID. 21816
- [46] Chaudhary, F.A., A. Iqbal, M.D. Khalid, N. Noor, J. Syed, M.N. Baig, O. Khattak, and S.U. Din, Validation and Reliability Testing of the Child Oral Impacts on Daily Performances (C-OIDP): Cross-Cultural Adaptation and Psychometric Properties in Pakistani School-Going Children. *Children-Basel*, 2022. 9(5): Article ID. 631
- [47] Kuppusamy, Y., R. Jayaseelan, G. Pandulu, V.S. Kumar, G. Murali, S. Dixit, and N.I. Vatin, Artificial Neural Network with a Cross-Validation Technique to Predict the Material Design of Eco-Friendly Engineered Geopolymer Composites. *Materials*, 2022. 15(10): Article ID. 3443
- [48] Minhas, H., A. Malik, D. Kurtz, Z. Fatiwala, F. Ahmed, F. Irfan, S. Lee, and Z. Esber, Cross-Validation of a Global Machine Learning Model to Predict COVID-19 Mortality. *American Journal of Respiratory and Critical Care Medicine*, 2022. 205
- [49] Ramirez, J., Unilateral sensorineural hearing loss identification based on double-density dual-tree complex wavelet transform and multinomial logistic regression. *Integrated Computer-Aided Engineering*, 2019. 26: p. 411-426